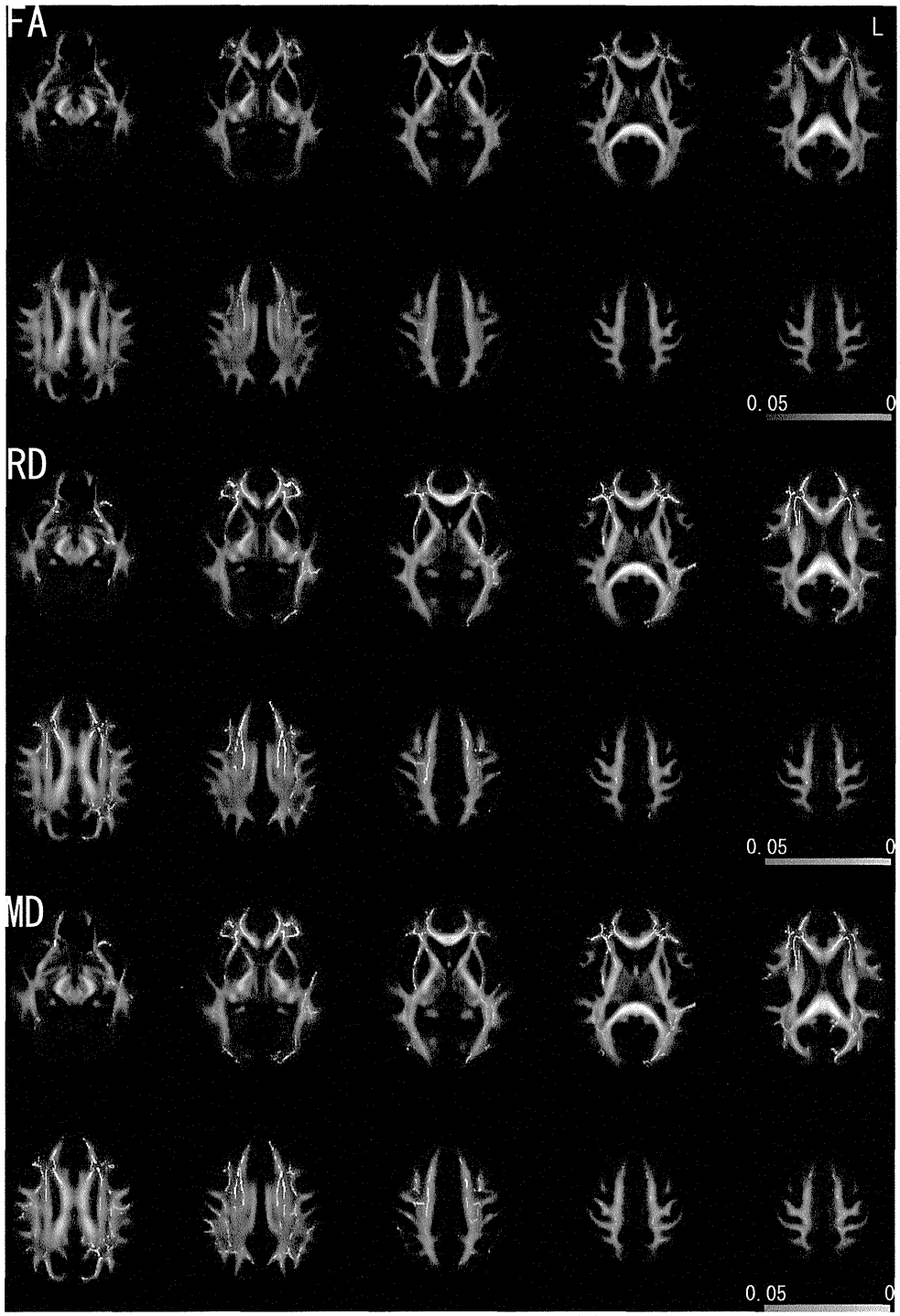


**Fig. 2.** Correlation between FA, RD, MD, and the CES-D score as identified by TBSS in female participants. The statistical image was thresholded at $P< 0.05$ and overlaid on the mean FA map of all participants. There were significant negative correlations between FA and the CES-D score (blue–light blue), and positive correlations between RD as well as MD and the CES-D score (red–yellow). L indicates left.

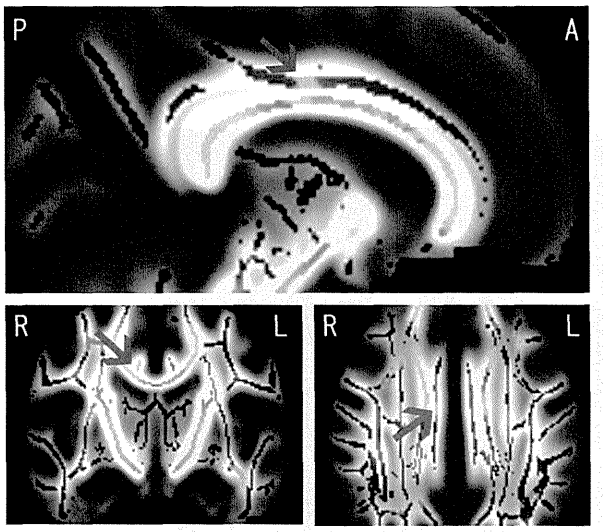


**Fig. 3.** Blue voxels show the regions where FA was reduced in association with the CES-D score in female participants ($P < 0.05$) overlaid on the mean FA skeleton (green voxels). The background image is the mean FA map of all participants. Arrows indicate the right dorsal anterior cingulate region (Talairach coordinates: $x = 6$, $y = -13$, $z = 28$). The same region was positively correlated with RD (not shown in this figure). A and P indicate anterior and posterior, and R and L indicate right and left, respectively.

at risk for depression, Huang et al. (2011) reported lower FA values in white matter tracts including the left cingulum in healthy adolescents at familial risk of unipolar depression than in controls. Some personality traits identified as predisposing factors for affective disorders have been reported to associate with white matter microstructures in widespread brain areas (Ayling et al., 2012; Bjørnebekk et al., 2013; Westlye et al., 2011). Bjørnebekk et al. (2013) demonstrated that increased neuroticism is associated with decreased FA, as well as increased MD and RD in widespread regions of white matter. These regions include the long association fibers connecting the frontal, occipital, parietal, and temporal lobes; tracts connecting orbitofrontal regions with limbic regions; fiber tracts connecting thalamic nuclei with the frontal lobes; and cross-hemispheric pathways, including the corpus callosum. These white matter microstructures may underlie vulnerability to depression, and the present study suggests that widespread regions of white matter are also associated with depressive symptoms in community-dwelling women. The affected regions are broader than regions of volume reduction, suggesting that microstructural changes in white matter precede reductions in brain volume. Note that we did not control for preclinical anxiety as a potential confound in this study. Because anxiety and depression are highly correlated, the results of the current study could have been modulated by comorbid preclinical anxiety. A more detailed analysis of the potential effect of anxiety is an important direction for future research.

### 4.3. Sex difference

In this study, depressive symptoms were associated with brain volume and white matter integrity only in female participants. One possible explanation of this is that the sex difference per se influences the brain structure in major depression (Frodl et al., 2002; Hastings et al., 2004) and even in subclinical depression. Another explanation is the heterogeneity of the participant's characteristics: the depressive symptoms measured by CES-D were statistically higher in women than in men. Therefore, the possibility remains that male participants who have the same depressive symptoms will show the same patterns in brain structure as females. Additional evidence from a more homogeneous group is needed to examine this possibility.

## 5. Conclusion

By using both VBM and TBSS in a large group of community-dwelling participants, we have shown associations between brain structures and depressive symptoms in female participants. Our findings show that frontal–limbic structures, including the bilateral anterior cingulate gyrus, are associated with depressive symptoms even at a subclinical level. Moreover, they show that white matter structure is associated with depressive symptoms in widespread regions.

## References

Abe, O., Yamasue, H., Kasai, K., Yamada, H., Aoki, S., Inoue, H. et al, 2010. Voxel-based analyses of gray/white matter volume and diffusion tensor data in major depression. Psychiatry Research 181, 64–70. http://dx.doi.org/10.1016/j.pscychresns.2009.07.007, 19959342.

Arfanakis, K., Haughton, V.M., Carew, J.D., Rogers, B.P., Dempsey, R.J., Meyerand, M.E., 2002. Diffusion tensor MR imaging in diffuse axonal injury. AJNR. American Journal of Neuroradiology 23, 794–802, 12006280.

Ayling, E., Aghajani, M., Fouche, J.-P., van, der Wee N., 2012. Diffusion tensor imaging in anxiety disorders. Current Psychiatry Reports 14, 197–202. http://dx.doi.org/10.1007/s11920-012-0273-z, 22460663.

Bjørnebekk, A., Fjell, A.M., Walhovd, K.B., Grydeland, H., Torgersen, S., Westlye, L.T., 2013. Neuronal correlates of the five factor model (FFM) of human personality: multimodal imaging in a large healthy sample. Neuroimage 65, 194–208. http://dx.doi.org/10.1016/j.neuroimage.2012.10.009, 23063449.

Boes, A.D., McCormick, L.M., Coryell, W.H., Nopoulos, P., 2008. Rostral anterior cingulate cortex volume correlates with depressed mood in normal healthy children. Biological Psychiatry 63, 391–397. http://dx.doi.org/10.1016/j.biopsych.2007.07.018, 17916329.

Botteron, K.N., Raichle, M.E., Drevets, W.C., Heath, A.C., Todd, R.D., 2002. Volumetric reduction in left subgenual prefrontal cortex in early onset depression. Biological Psychiatry 51, 342–344. http://dx.doi.org/10.1016/S0006-3223(01)01280-X, 11958786.

Bremner, J.D., Vythilingam, M., Vermetten, E., Nazeer, A., Adil, J., Khan, S. et al, 2002. Reduced volume of orbitofrontal cortex in major depression. Biological Psychiatry 51, 273–279. http://dx.doi.org/10.1016/S0006-3223(01)01336-1, 11958777.

Caetano, S.C., Kaur, S., Brambilla, P., Nicoletti, M., Hatch, J.P., Sassi, R.B. et al, 2006. Smaller cingulate volumes in unipolar depressed patients. Biological Psychiatry 59, 702–706. http://dx.doi.org/10.1016/j.biopsych.2005.10.011, 16414029.

Campbell, S., Marriott, M., Nahmias, C., MacQueen, G.M., 2004. Lower hippocampal volume in patients suffering from depression: a meta-analysis. American Journal of Psychiatry 161, 598–607. http://dx.doi.org/10.1176/appi.ajp.161.4.598, 15056502.

Cuijpers, P., de Graaf, R., van Dorsselaer, S., 2004. Minor depression: risk profiles, functional disability, health care use and risk of developing major depression. Journal of Affective Disorders 79, 71–79. http://dx.doi.org/10.1016/S0165-0327(02)00348-8, 15023482.

Dotson, V.M., Davatzikos, C., Kraut, M.A., Resnick, S.M., 2009. Depressive symptoms and brain volumes in older adults: a longitudinal magnetic resonance imaging study. Journal of Psychiatry & Neuroscience : JPN 34, 367–375, 19721847.

Egger, K., Schocke, M., Weiss, E., Auffinger, S., Esterhammer, R., Goebel, G. et al, 2008. Pattern of brain atrophy in elderly patients with depression revealed by voxel-based morphometry. Psychiatry Research 164, 237–244. http://dx.doi.org/10.1016/j.pscychresns.2007.12.018, 19013058.

Fazekas, F., Chawluk, J.B., Alavi, A., Hurtig, H.I., Zimmerman, R.A., 1987. MR signal abnormalities at 1.5 T in Alzheimer's dementia and normal aging. American Journal of Roentgenology 149, 351–356. http://dx.doi.org/10.2214/ajr.149.2.351.

Frodl, T., Meisenzahl, E.M., Zetzsche, T., Born, C., Groll, C., Jäger, M., et al. 2002. Hippocampal changes in patients with a first episode of major depression. American Journal of Psychiatry 159, 1112–1118. http://dx.doi.org/10.1176/appi.ajp.159.7.1112, 12091188.

Grucza, R.A., Przybeck, T.R., Spitznagel, E.L., Cloninger, C.R., 2003. Personality and depressive symptoms: a multi-dimensional analysis. Journal of Affective Disorders 74, 123–130. http://dx.doi.org/10.1016/S0165-0327(02)00303-8, 12706513.

Harsan, L.A., Poulet, P., Guignard, B., Steibel, J., Parizel, N., de Sousa, P.L. et al, 2006. Brain dysmyelination and recovery assessment by noninvasive in vivo diffusion tensor magnetic resonance imaging. Journal of Neuroscience Research 83, 392–402, 16397901.

Hastings, R.S., Parsey, R.V., Oquendo, M.A., Arango, V., Mann, J.J., 2004. Volumetric analysis of the prefrontal cortex, amygdala, and hippocampus in major depression. Neuropsychopharmacology : Official Publication of the American College of Neuropsychopharmacology 29, 952–959. http://dx.doi.org/10.1038/sj.npp.1300371, 14997169.

Haringsma, R., Engels, G.I., Beekman, A.T., Spinhoven, P., 2004. The criterion validity of the Center for Epidemiological Studies Depression Scale (CES-D) in a sample of self-referred elders with depressive symptomatology. International Journal of Geriatric Psychiatry 19, 558–563. http://dx.doi.org/10.1002/gps.1130, 15211536.

Hayakawa, Y.K., Sasaki, H., Takao, H., Mori, H., Hayashi, N., Kunimatsu, A. et al, 2013. Structural brain abnormalities in women with subclinical depression, as revealed by voxel-based morphometry and diffusion tensor imaging. Journal of Affective Disorders 144, 263–268. http://dx.doi.org/10.1016/j.jad.2012.10.023,

23141669.
Huang, H., Fan, X., Williamson, D.E., Rao, U., 2011. White matter changes in healthy adolescents at familial risk for unipolar depression: a diffusion tensor imaging study. Neuropsychopharmacology: Official Publication of the American College of Neuropsychopharmacology 36, 684–691. http://dx.doi.org/10.1038/npp.2010.199, 21085111.
Jovicich, J., Czanner, S., Greve, D., Haley, E., van, der Kouwe A., Gollub, R. et al, 2006. Reliability in multi-site structural MRI studies: effects of gradient non-linearity correction on phantom and human data. Neuroimage 30, 436–443. http://dx.doi.org/10.1016/j.neuroimage.2005.09.046, 16300968.
Kieseppä, T., Eerola, M., Mäntylä, R., Neuvonen, T., Poutanen, V.P., Luoma, K. et al, 2010. Major depressive disorder and white matter abnormalities: a diffusion tensor imaging study with tract-based spatial statistics. Journal of Affective Disorders 120, 240–244. http://dx.doi.org/10.1016/j.jad.2009.04.023, 19467559.
Lavretsky, H., Kumar, A., 2002. Clinically significant non-major depression: old concepts, new insights. American Journal of Geriatric Psychiatry: Official Journal of the American Association for Geriatric Psychiatry 10, 239–255. http://dx.doi.org/10.1176/appi.ajgp.10.3.23910.1097/00019442-200205000-00003, 11994211.
Lorenzetti, V., Allen, N.B., Fornito, A., Yücel, M., 2009. Structural brain abnormalities in major depressive disorder: a selective review of recent MRI studies. Journal of Affective Disorders 117, 1–17. http://dx.doi.org/10.1016/j.jad.2008.11.021, 19237202.
Lyness, J.M., King, D.A., Cox, C., Yoediono, Z., Caine, E.D., 1999. The importance of subsyndromal depression in older primary care patients: prevalence and associated functional disability. Journal of the American Geriatrics Society 47, 647–652, 10366161.
Nichols, T.E., Holmes, A.P., 2002. Nonparametric permutation tests for functional neuroimaging: a primer with examples. Human Brain Mapping 15, 1–25. http://dx.doi.org/10.1002/hbm.1058, 11747097.
Pujol, J., López, A., Deus, J., Cardoner, N., Vallejo, J., Capdevila, A. et al, 2002. Anatomical variability of the anterior cingulate gyrus and basic dimensions of human personality. NeuroImage 15, 847–855. http://dx.doi.org/10.1006/nimg.2001.1004, 11906225.
Radloff, L.S., 1977. The CES-D Scale:a self-report depression scale for research in the general population. Applied Psychological Measurement 1, 386–401.
Shimony, J.S., Sheline, Y.I., D'Angelo, G., Epstein, A.A., Benzinger, T.L., Mintun, M.A. et al, 2009. Diffuse microstructural abnormalities of normal-appearing white matter in late life depression: a diffusion tensor imaging study. Biological Psychiatry 66, 245–252. http://dx.doi.org/10.1016/j.biopsych.2009.02.032, 19375071.
Smith, S.M., 2002. Fast robust automated brain extraction. Human Brain Mapping 17, 143–155. http://dx.doi.org/10.1002/hbm.10062, 12391568.
Smith, S.M., Jenkinson, M., Woolrich, M.W., Beckmann, C.F., Behrens, T.E., Johansen-Berg, H. et al, 2004. Advances in functional and structural MR image analysis and implementation as FSL. Neuroimage 23 (Suppl 1), S208–S219. http://dx.doi.org/10.1016/j.neuroimage.2004.07.051, 15501092.
Smith, S.M., Jenkinson, M., Johansen-Berg, H., Rueckert, D., Nichols, T.E., Mackay, C.E. et al, 2006. Tract-based spatial statistics: voxelwise analysis of multi-subject diffusion data. Neuroimage 31, 1487–1505. http://dx.doi.org/10.1016/j.neuroimage.2006.02.024, 16624579.
Smith, S.M., Nichols, T.E., 2009. Threshold-free cluster enhancement: addressing problems of smoothing, threshold dependence and localisation in cluster inference. Neuroimage 44, 83–98. http://dx.doi.org/10.1016/j.neuroimage.2008.03.061, 18501637.
Song, S.K., Sun, S.W., Ramsbottom, M.J., Chang, C., Russell, J., Cross, A.H., 2002. Dysmyelination revealed through MRI as increased radial (but unchanged axial) diffusion of water. Neuroimage 17, 1429–1436. http://dx.doi.org/10.1006/nimg.2002.1267, 12414282.
Song, S.K., Sun, S.W., Ju, W.K., Lin, S.J., Cross, A.H., Neufeld, A.H., 2003. Diffusion tensor imaging detects and differentiates axon and myelin degeneration in mouse optic nerve after retinal ischemia. NeuroImage 20, 1714–1722. http://dx.doi.org/10.1016/j.neuroimage.2003.07.005, 14642481.
Song, S.K., Yoshino, J., Le, T.Q., Lin, S.J., Sun, S.W., Cross, A.H. et al, 2005. Demyelination increases radial diffusivity in corpus callosum of mouse brain. Neuroimage 26, 132–140. http://dx.doi.org/10.1016/j.neuroimage.2005.01.028, 15862213.
Videbech, P., Ravnkilde, B., 2004. Hippocampal volume and depression: a meta-analysis of MRI studies. American Journal of Psychiatry 161, 1957–1966. http://dx.doi.org/10.1176/appi.ajp.161.11.1957, 15514393.
Westlye, L.T., Bjørnebekk, A., Grydeland, H., Fjell, A.M., Walhovd, K.B., 2011. Linking an anxiety-related personality trait to brain White matter microstructure. Archives of General Psychiatry 68, 369–377. http://dx.doi.org/10.1001/archgenpsychiatry.2011.24, 21464361.
Wozniak, J.R., Lim, K.O., 2006. Advances in white matter imaging: a review of in vivo magnetic resonance methodologies and their applicability to the study of development and aging. Neuroscience and Biobehavioral Reviews 30, 762–774. http://dx.doi.org/10.1016/j.neubiorev.2006.06.003, 16890990.

# Cerebral Hemodynamic Impairment: Assessment with Resting-State Functional MR Imaging[1]

Shiori Amemiya, MD, PhD
Akira Kunimatsu, MD, PhD
Nobuhito Saito, MD, PhD
Kuni Ohtomo, MD, PhD

**Purpose:** To test the feasibility of noninvasive global assessment of cerebral hemodynamic impairment with use of resting-state blood oxygenation level–dependent functional magnetic resonance (MR) imaging.

**Materials and Methods:** In this institutional review board–approved study, five patients with chronic hypoperfusion without neurologic impairment and six patients with acute stroke underwent 10-minute resting-state functional MR imaging and dynamic susceptibility-weighted contrast-enhanced perfusion MR imaging, which was considered the standard of reference. All patients gave informed consent. The temporal shift of low-frequency signal fluctuations in each voxel compared with the averaged whole brain or global mean signal at resting-state functional MR imaging and the delay in time to peak at dynamic susceptibility-weighted contrast-enhanced perfusion imaging were computed with voxel-wise analysis. The similarity of the temporal delay maps obtained with resting-state functional MR imaging and perfusion data, as well as the stability of the resting-state functional MR imaging measurement, were evaluated with the Dice similarity coefficient (DSC) and the two-tailed $t$ test (random-effect analysis).

**Results:** The brain tissue with normal perfusion at dynamic susceptibility-weighted contrast-enhanced imaging showed no delay to global mean signal at resting-state functional MR imaging, whereas areas of abnormal perfusion with delayed time to peak (3.4 seconds ± 2.1) showed a delay at resting-state functional MR imaging that was similar to the time to peak at dynamic susceptibility-weighted contrast-enhanced perfusion imaging, both in spatial coverage (mean DSC, 0.57 ± 0.16) and tendency ($t = 5.1$, $P < .001$). Resting-state functional MR imaging measurements were highly stable (mean DSC, 0.83 ± 0.12).

**Conclusion:** Resting-state functional MR imaging temporal-shift analysis can noninvasively demonstrate the extent and degree of perfusion delay in patients with hypoperfusion both with and without neurologic deficit.



[1] From the Departments of Radiology (S.A., A.K., K.O.) and Neurosurgery (N.S.), Graduate School of Medicine, University of Tokyo, 7-3-1 Hongo, Bunkyo-ku, Tokyo, 113-8655, Japan. Received April 29, 2013; revision requested June 17; revision received July 9; accepted July 19; final version accepted July 31. **Address correspondence to** S.A. (e-mail: *amemiya-tky@umin.ac.jp*).

Effective prevention and protection from irreversible infarction forms the basis of the treatments in cerebral ischemic diseases. Identification of salvageable, hypoperfused tissue at risk for future infarction by assessing cerebral perfusion plays a key role in patient selection for revascularization or reperfusion therapies in chronic and acute ischemic diseases (1). Although most clinical perfusion imaging entails exogenous contrast material or tracers, noninvasive methods that exploit endogenous contrast material, including blood oxygenation level–dependent imaging, are emerging as a potential substitute (2) to overcome limitations associated with adverse effects of the contrast material, technical issues, or cost.

Blood oxygenation level–dependent imaging is used to infer neuronal activity in functional magnetic resonance (MR) imaging; however, it is also sensitive to local background hemodynamics and thus is applicable to the evaluation of cerebrovascular impairment when temporal shift reflecting background vascular delay is evaluated under a task-controlled, time-locked condition (3,4). The drawback of the approach is that an assessable region is limited to task-specific activation areas. To overcome this limitation, we further applied resting-state functional MR imaging to global hemodynamic assessment. Although resting-state functional MR imaging is commonly used to investigate synchronous neuronal activity that occurs in the absence of explicit task performance (5,6), recent investigations also suggest that temporal dynamics of low-frequency fluctuations can indicate propagation of bulk blood flow (7,8).

In the present study, we evaluated the temporal shift of low-frequency fluctuations to global mean or averaged whole-brain signal, which is the most prominent and spatially ubiquitous component of resting-state functional MR imaging (9,10). Given a notion that the major source of the component is nonneuronal physiologic fluctuations related to respiration and cardiac pulsation (11,12), it was hypothesized that the measurement reflects temporal dynamics of underlying vasculature. Both patients with chronic hypoperfusion without neural impairment and patients with acute stroke were investigated to test the hypothesis that the source of the temporal shift is vascular rather than neuronal in origin. The results were compared with those from dynamic susceptibility-weighted contrast material–enhanced perfusion-weighted MR imaging in the areas of abnormal perfusion showing delayed time to peak compared with the corresponding contralateral region. The similarity of the temporal delay at resting-state functional MR imaging and the time to peak at perfusion imaging, as well as stability of the resting-state functional MR imaging measurement, were evaluated to explore the implication, potential, and limitation of the resting-state functional MR imaging approach. The purpose of this study was to test the feasibility of noninvasive global assessment of cerebral hemodynamic impairment with use of resting-state functional MR imaging.

### Advances in Knowledge

- Areas of abnormal cerebral perfusion with delayed time to peak at dynamic susceptibility-weighted contrast-enhanced perfusion MR imaging show similar delays at resting-state functional MR imaging, both in extent and in tendency ($t = 5.1$, $P < .001$).
- The resting-state functional MR imaging temporal-shift analysis can extract signal delay that is vascular rather than neuronal in origin and, hence, is applicable to the assessment of hemodynamic impairment in patients with hypoperfusion both with and without neurologic deficit.

### Implication for Patient Care

- By exploiting endogenous blood oxygenation level–dependent contrast, resting-state functional MR imaging temporal analysis can noninvasively demonstrate the extent and degree of perfusion delay in patients with hypoperfusion both with and without neurologic deficit.

## Materials and Methods

### Patients

From December 2011 to December 2012, five patients with chronic hypoperfusion (patients C1–C5) and six patients with acute stroke (patients A1–A6) (seven men; mean age ± standard deviation, 62 years ± 19) who met the following inclusion criteria were prospectively included in the study. Patients with chronic hypoperfusion were included in this study if they *(a)* had long-standing unilateral occlusion of the middle cerebral artery, *(b)* were free of neuronal functional impairment, and *(c)* had no structural destruction due to hypoperfusion or other diseases. Patients with acute stroke were included if contrast material–enhanced MR imaging was feasible within 1 day from symptom onset (16, 10, 22, 17, 16, 6 hours, respectively). Patients were excluded if they had severe head motion larger than 5 mm, which excluded one patient with acute stroke (patient A6). Two of the five patients with chronic hypoperfusion (patients C2 and C5) had had an episode of weakness in the contralateral extremities that fully recovered without any treatment. The other three patients were asymptomatic, and the occlusion was incidentally found at screening MR examination. Therefore, the patients with chronic hypoperfusion

**Published online before print**
10.1148/radiol.13130982 **Content code:** NR

**Radiology 2014;** 270:548–555

**Abbreviation:**
DSC = Dice similarity coefficient

**Author contributions:**
Guarantor of integrity of entire study, S.A.; study concepts/study design or data acquisition or data analysis/interpretation, all authors; manuscript drafting or manuscript revision for important intellectual content, all authors; manuscript final version approval, all authors; literature research, S.A.; clinical studies, S.A.; statistical analysis, S.A.; and manuscript editing, S.A., A.K., K.O.

Conflicts of interest are listed at the end of this article.

**Summary of Patient Data**

| Patient No./Age (y)/Sex | Diagnosis | Volume of Areas of Delayed Perfusion (mL) | | Overlap* | Stability† | Head Displacement (mm) | | Diffusion-weighted Imaging Coverage‡ |
|---|---|---|---|---|---|---|---|---|
| | | RS Functional MR Imaging | Perfusion MR Imaging | | | Mean | Maximum | |
| C1/64/F | L MCA occlusion | 332.7 | 365.1 | 0.66 | 0.85/0.75 | 0.16 | 0.50 | NA |
| C2/58/M | R MCA occlusion | 227.0 | 382.5 | 0.70 | 0.93/0.89 | 1.23 | 2.31 | NA |
| C3/74/M | R MCA occlusion§ | 102.9 | 370.3 | 0.31 | NA | 0.67 | 1.06 | NA |
| C4/39/F | L MCA occlusion | 271.0 | 356.5 | 0.55 | 0.76/0.82 | 0.20 | 0.77 | NA |
| C5/21/F | L MCA occlusion§ | 150.0 | 337.0 | 0.38 | 0.82/0.7 | 0.40 | 0.78 | NA |
| A1/49/M | R MCA infarction§ | 204.8 | 345.1 | 0.52 | 0.88/0.91 | 0.42 | 1.55 | 0.58 |
| A2/72/M | R PCA/SCA infarction§ | 138.3 | 121.9 | 0.74 | 0.98/0.92 | 0.57 | 1.19 | 0.90 |
| A3/69/M | R PICA infarction‖ | 42.6 | 77.0 | 0.49 | 0.83/0.89 | 0.50 | 0.78 | 0.002 |
| A4/82/M | R MCA/ACA infarction | 410.5 | 284.9 | 0.75 | 0.93/0.83 | 0.13 | 0.22 | 0.72 |
| A5/73/F | R ACA infarction§ | 152.1 | NA | NA | 0.71/0.49 | 0.20 | 0.69 | 0.97 |

Note.—ACA = anterior cerebral artery, L = left, MCA = middle cerebral artery, NA = not applicable, PCA = posterior cerebral artery, PICA = posterior inferior cerebellar artery, R = right, RS = resting-state, SCA = superior cerebellar artery.

* Data are DSCs.

† Data are DSCs for all data versus first 5 minutes and all data versus last 5 minutes, respectively.

‡ Fraction of areas with diffusion restriction covered with resting-state functional MR imaging delay.

§ A minor contralateral lesion was also present.

‖ Hemorrhagic core.

did not have true ischemia. Informed consent was obtained from all participants before imaging. All procedures were in compliance with the Declaration of Helsinki, and the institutional review board of the University of Tokyo approved the study.

### Data Acquisition

Ten-minute resting-state functional MR imaging and dynamic susceptibility-weighted contrast-enhanced perfusion imaging—in addition to routine MR imaging examinations that included diffusion-weighted, high-spatial-resolution T1-weighted, T2-weighted, T2*-weighted, and fluid-attenuated inversion-recovery MR imaging and MR angiography—were performed with a whole-body 3.0-T MR unit (Signa HDx; GE Healthcare, Milwaukee, Wis) by using a 12-channel phased-array head coil, with single-shot gradient-echo echo-planar imaging for functional MR imaging and perfusion-weighted imaging and single-shot spin-echo echo-planar imaging for diffusion-weighted imaging. Imaging parameters for resting-state functional MR imaging were as follows: 2000/30 (repetition time msec/echo time msec), 90° flip angle, 64 × 64 matrix, 240 × 240-mm field of view, 4-mm-thick sections, no gap, 40 sections, and 304 frames. Imaging parameters for diffusion-weighted imaging were as follows: 6500/74, 90° flip angle, 128 × 192 matrix, 210 × 210-mm field of view, 5-mm-thick sections, 1-mm gap, 25 sections, and $b = 0$ and 1000 sec/mm$^2$ in three orthogonal directions. Perfusion-weighted imaging could not be performed in patient A5 owing to a decline in her physical condition. Resting-state functional MR imaging was shortened to 5 minutes in patient C3 because of time restriction.

### Data Analysis

Functional MR imaging data were processed with SPM 5 software (*http://www.fil.ion.ucl.ac.uk/spm/software/spm5/*) and in-house scripts written and implemented in Matlab R2009a (MathWorks, Natick, Mass) (S.A., with 4 years of experience in functional MR imaging data analysis). The first four volumes were discarded to allow for T1 equilibration effects. Data were realigned to the first volume to account for movement artifact, corrected for differences in acquisition time between sections, spatially normalized to standard Montreal Neurologic Institute stereotaxic coordinates, spatially smoothed with a Gaussian kernel with 8-mm full width at half maximum, linearly detrended, and band-pass filtered at 0.01–0.1 Hz. The temporal shift that gives the best positive fit among the Pearson correlation coefficients between each voxel's signal time course and time-shifted (±20 seconds) global mean signal in the unaffected hemisphere was computed with voxel-wise analysis (Fig 1). Regions of abnormal perfusion delay were determined within anterior or posterior circulation territories that were defined by using WFU Pick Atlas 2.4 (*http://fmri.wfubmc.edu/software/PickAtlas*) by subtracting each mirror-reversed time-to-peak map from the original. The automatic process eliminates manual definition of regions of interest that could suffer from low intra- and interobserver repeatability. The mean transit time in the affected area was also computed

**Figure 1**

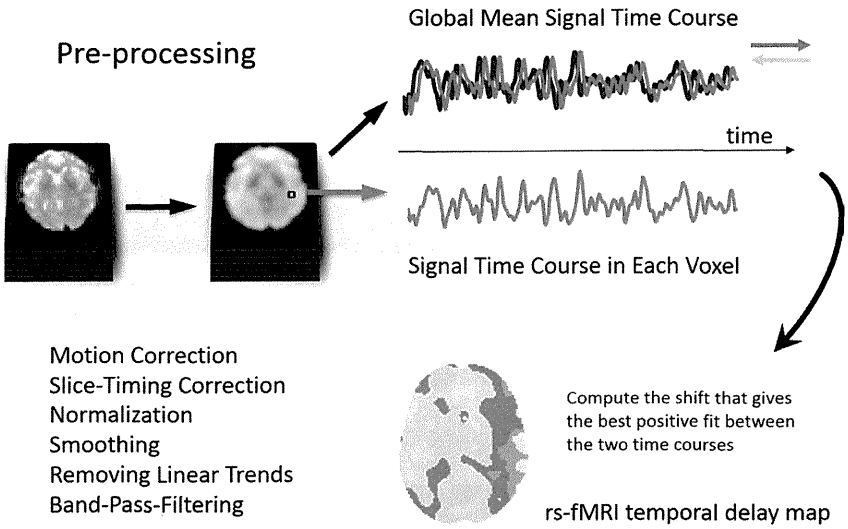


**Figure 1:** Schematic of resting-state functional MR imaging *(rs-fMRI)* data processing. After preprocessing, which included realignment, section timing correction, normalization, spatial smoothing, removal of linear trends, and band-pass filtering, temporal shift that gives the best positive fit among correlation coefficients between each voxel's signal time course and time-shifted (±20 seconds) global signal in the unaffected hemisphere was computed with voxel-wise analysis.

**Figure 2**

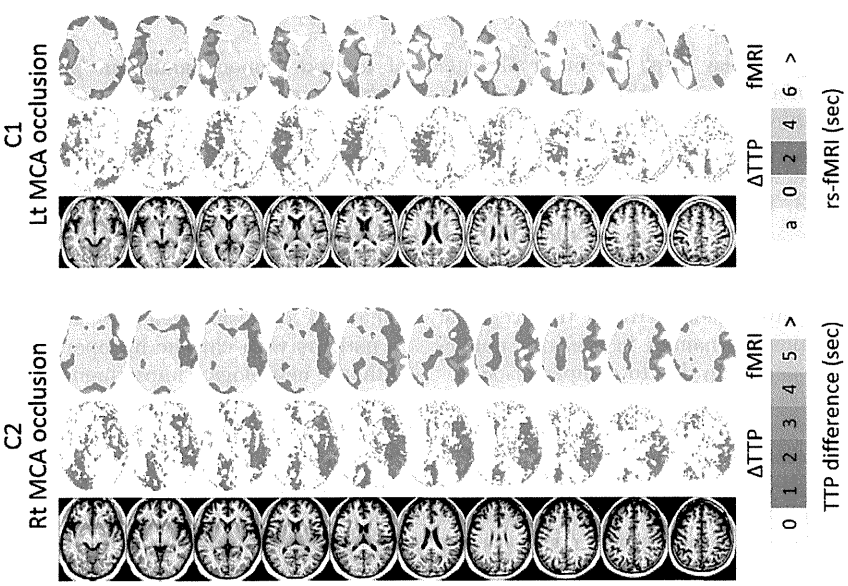


**Figure 2:** Comparison of temporal shift on resting-state functional MR images *(rs-fMRI)* and perfusion time-to-peak *(TTP)* difference on dynamic susceptibility-weighted contrast-enhanced perfusion MR images in patients with chronic hypoperfusion (patients C1 and C2). Areas of abnormal perfusion with delayed time to peak compared with corresponding contralateral region (middle rows) show delay at temporal-shift analysis of resting-state functional MR images (top rows). Delayed areas at resting-state functional MR imaging also included large veins and venous sinuses. T1-weighted MR images (bottom rows) are shown for anatomic reference. *a* = advanced, *Lt* = left, *MCA* = middle cerebral artery, *Rt* = right.

with delay-insensitive block-circulant singular-value decomposition deconvolution (13) by using PMA 3.4 (*http://asist.umin.jp/index-e.htm*).

Temporal maps from resting-state functional MR imaging were compared with perfusion data by computing the Dice similarity coefficient (DSC) for the assessment of lesion extent (spatial overlap). The similarity of the tendency of the two measurements was also assessed by computing correlation coefficients between resting-state functional MR imaging delay and time-to-peak maps over the whole-brain voxels that were transformed to Fisher $z$ and tested by using a two-tailed $t$ test over subjects (random-effects analysis) against the null hypothesis of no correlation. Stability of the resting-state functional MR imaging measurement was assessed by computing DSC between delay maps obtained from 10-minute data and those obtained from first- or last 5-minute data, respectively.

For data in patients with acute stroke, resting-state functional MR imaging delay coverage was computed within the infarction core that was automatically determined on the basis of a dual threshold: an absolute threshold of apparent diffusion coefficient of less than $615 \times 10^{-6}$ mm$^2$/sec and a relative threshold of signal intensity of more than mean +1.5 standard deviations in $b$ = 1000 images (14).

## Results

### Characteristics of Temporal Shift at Resting-State Functional MR Imaging

The brain tissue with normal perfusion showed no delay to global mean signal, whereas areas of abnormal perfusion with delayed time to peak (mean, 3.4 seconds ± 2.1) showed a delay at resting-state functional MR imaging (Fig 2, Table). Areas showing delays at resting-state functional MR imaging (mean, 2.3 seconds ± 1.3) also included large veins and venous sinuses, where time to peak is generally delayed (Figs 2, 3). Averaged signal time course in delayed voxels plotted against the global mean

signal is shown in Figure 4, *A*. Positive correlation between averaged signal time course in each delayed region grouped according to the temporal shift and time-shifted global mean signal also ensures that the delay is actually delay and not reflecting negative correlation (Fig 4, *B*).

### Similarity between Temporal Delay at Resting-State Functional MR Imaging and Time to Peak at Dynamic Susceptibility-weighted Contrast-enhanced Perfusion Imaging

Spatial overlap of the two measurements was computed as DSC (mean DSC, 0.57 ± 0.16; range, 0.31–0.75) (Table). Although the coverage with resting-state functional MR imaging was smaller than that measured with perfusion time to peak ($P < .03$, $t = 2.8$), the overlap was higher when the hypoperfusion was limited to a unilateral hemisphere (DSC, 0.49–0.75) (Table). The two temporal measurements also showed significant similarity in tendency across whole-brain voxels over the subjects; that is, greater delay in one map corresponds to greater delay in the other (random-effect analysis: $t = 5.1$, $P < .001$). The mean transit time in the areas of abnormal perfusion was also increased (mean, 0.76 second ± 0.67).

### Stability of the Resting-State Functional MR Imaging Measurement

The resting-state functional MR imaging temporal measurement was highly stable, and similar maps could be repeatedly obtained from the first or last half of the whole 10-minute data in all patients (mean DSC, 0.83 ± 0.12) (Fig 5, Table).

### Resting-State Functional MR Imaging Measurement in Acute Stroke

In patients with acute stroke, the temporal map obtained at resting-state functional MR imaging did not reveal delay in the areas with diffusion restriction in a patient with a hemorrhagic core (patient A3), who was examined 22 hours from symptom onset (Table). However, a large portion of the core showed resting-state functional MR imaging delay in all the other patients examined at an early time from onset (fraction of areas with diffusion restriction covered with resting-state functional MR imaging delay = 0.79 ± 0.18; Fig 3, Table).

**Figure 3**

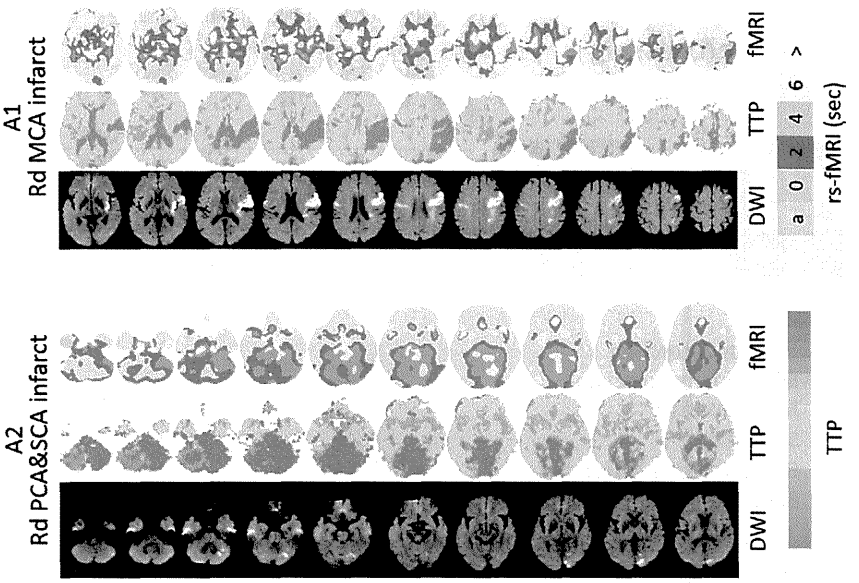


**Figure 3:** Comparison of temporal shift on resting-state functional MR images (*rs-fMRI*, top rows) and time to peak (*TTP*) on dynamic susceptibility-weighted contrast-enhanced perfusion images (middle rows) in patients with acute stroke (patients A1 and A2). Diffusion-weighted images (bottom rows) are also shown. Areas with diffusion restriction are covered with resting-state functional MR imaging delay. *a* = advanced, *MCA* = middle cerebral artery, *PCA* = posterior cerebellar artery, *Rd* = right dominant, *SCA* = superior cerebellar artery.

## Discussion

Our study demonstrates that regional temporal dynamics in areas of abnormal perfusion due to compromised hemodynamics can be assessed with resting-state functional MR imaging in both patients with chronic hypoperfusion and those with acute stroke. Resting-state functional MR imaging–derived temporal data were similar to perfusion time-to-peak measurement both in extent and tendency, and the measurement was highly stable. The results are in line with those from recent studies that showed that blood oxygen level–dependent functional MR imaging is applicable not only to the assessment of neuronal function but also to the evaluation of altered hemodynamics in patients with hypoperfusion (3,4,15) and may shed light on the underlying cause of the signal temporal shift at resting-state functional MR imaging.

The similarity between the temporal shift at resting-state functional MR imaging and the time to peak at dynamic susceptibility-weighted contrast-enhanced perfusion-weighted imaging in patients with chronic hypoperfusion without neurologic impairment provides corroborative evidence suggesting that the origin of the resting-state functional MR imaging delay is vascular but not neurologic deficit, which is well accorded with the results of concurrent near-infrared spectroscopy and functional MR imaging studies showing that temporal dynamics at resting-state functional MR imaging can reflect propagation of physiologic fluctuations in healthy subjects (7,8).

One recent study in patients with acute stroke reported that resting-state functional MR imaging signal is

**Figure 4**

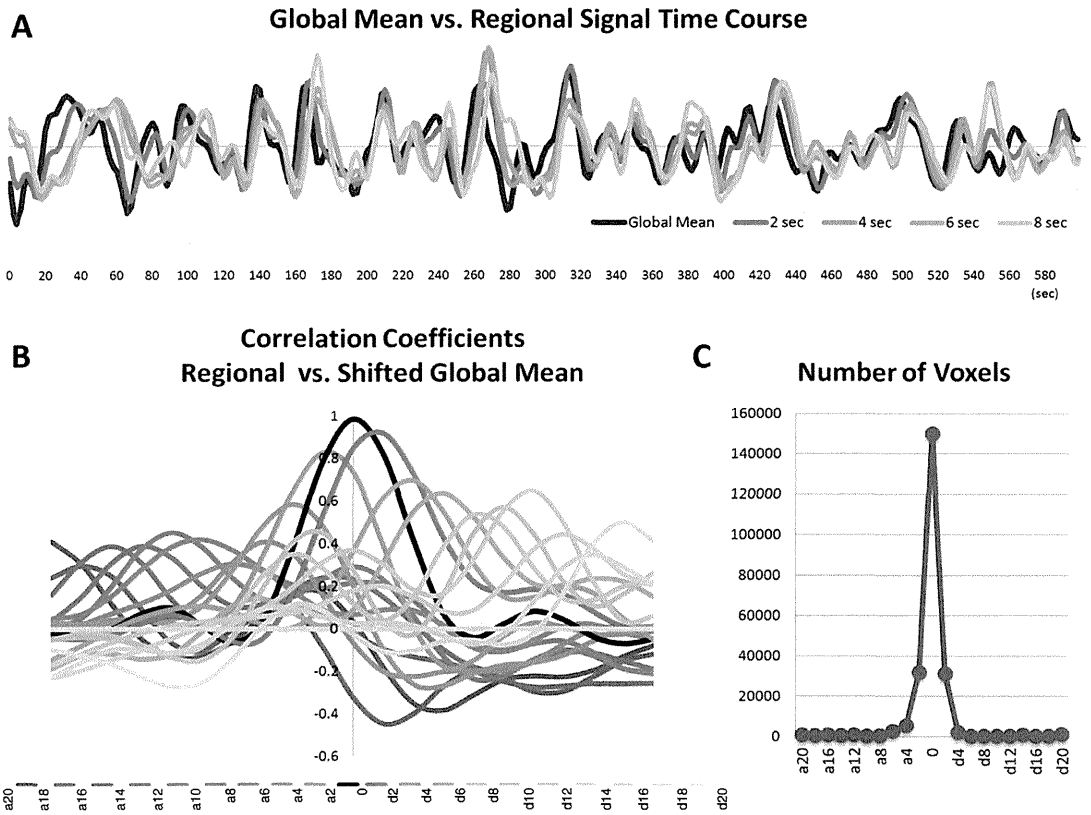


**Figure 4:** Global mean and delayed signal time course, correlation coefficients, and number of voxels for each shift. *A*, Averaged signal time course in 2–8-second delayed voxels is plotted against global mean signal. *B*, Correlation coefficients between averaged signal time course in each region grouped according to temporal shift and time-shifted global mean signal were also plotted to ensure that delay is actually delay and does not reflect negative correlation. *C*, Most voxels showed no delay to global mean signal. *a2–a20* = 2–20 seconds advanced, *d2–d20* = 2–20 seconds delayed compared with global mean.

delayed in the diffusion-perfusion mismatch area, but not in the core (15), leaving open the possibility of neuronal involvement because perfusion is commonly delayed in acute stroke core when evaluated in the acute hypoperfused stage. Although the ischemic penumbra was originally defined as a region of reduced blood flow that causes absent spontaneous neuronal activity but with sufficient energy remaining for ion pumping (16), the MR imaging–defined ischemic penumbra does not necessarily coincide with this definition and part of the perfusion abnormality can represent oligemic tissue with sustained neuronal activity that might have corresponded to the delayed area in their study.

In our study, we showed that resting-state functional MR imaging delay was also demonstrated in nonhemorrhagic infarction core areas of ischemia where the normal spontaneous neuronal activity must be absent. The finding not only reinforces the hypothesis that the delay is vascular in origin but also supports the idea that the major source of the signal fluctuations evaluated in the analysis is nonneuronal, which implies in practical terms that the resting-state functional MR imaging temporal analysis no more differentiates oligemia from ischemia than perfusion imaging does.

Likewise, the resting-state functional MR imaging temporal-shift analysis also has limitations similar to those of perfusion imaging (eg, vulnerability to head motion or vascular damage), which can theoretically reduce the source of signal (flow and volume of vessels), whether vascular or neuronal in origin, against the background noise. Another limitation is that the resting-state functional MR imaging delay map is variable depending on the extent of the ischemic lesion, which holds true for any approach in which relative measurements are used.

Nonetheless, noninvasiveness, simplicity, high stability, wide availability, and lower cost of the resting-state functional MR imaging measurement are all attractive for clinical use because cerebral ischemia remains a common disease—with a prevalence of up to

2.8% in the United States (17). A noninvasive approach is also suitable for repetitive follow-up examinations to monitor longitudinal progression over time and would be even more beneficial for patients with contraindications to nephrotoxic contrast material or when subsequent endovascular intervention is considered as a treatment option.

In conclusion, we confirmed that temporal dynamics in areas of abnormal perfusion due to compromised hemodynamics can be assessed with resting-state functional MR imaging. The temporal shift at resting-state functional MR imaging under hypoperfusion or ischemia reflects delay that is vascular in origin and, hence, is applicable to the noninvasive assessment of hemodynamic impairment in patients with hypoperfusion both with and without neurologic deficit.

**Acknowledgments:** We thank the members of the Department of Radiology, division of Diagnosis, and of the Department of Neurosurgery at the University of Tokyo Hospital for their support in conducting the study.

**Disclosures of Conflicts of Interest: S.A.** No relevant conflicts of interest to disclose. **A.K.** Financial activities related to the present article: none to disclose. Financial activities not related to the present article: institution has grants/grants pending with Bayer Healthcare; receives payment for lectures including service on speakers bureaus from Bayer Healthcare, Eisai, Daiichi-Sankyo Healthcare, and GE Healthcare. Other relationships: none to disclose. **N.S.** No relevant conflicts of interest to disclose. **K.O.** Financial activities related to the present article: none to disclose. Financial activities not related to the present article: institution has grants/grants pending from Daiichi-Sankyo Healthcare. Other relationships: none to disclose.

**Figure 5**

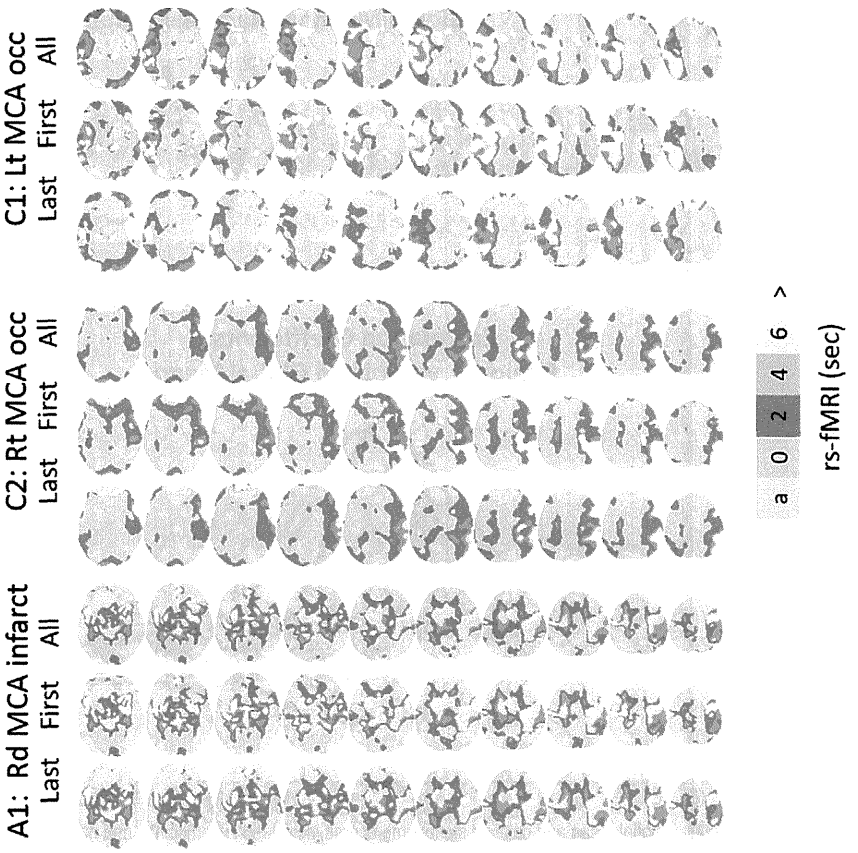


**Figure 5:** Stability of resting-state functional MR imaging *(rs-fMRI)* measurement. Resting-state functional MR imaging temporal maps were highly stable, and similar maps were obtained from first or last half of whole 10-minute data (patient C1: DSC = 0.85 for all data vs first 5 minutes and 0.75 for all data vs last 5 minutes; patient C2: DSC = 0.93 for all data vs first 5 minutes and 0.89 for all data vs last 5 minutes; patient A1: DSC = 0.88 for all data vs first 5 minutes and 0.91 for all data vs last 5 minutes). *a* = advanced, *Lt* = left, *MCA* = middle cerebral artery, *occ* = occlusion, *Rd* = right dominant, *Rt* = right.

## References

1. Latchaw RE, Yonas H, Hunter GJ, et al. Guidelines and recommendations for perfusion imaging in cerebral ischemia: a scientific statement for healthcare professionals by the writing group on perfusion imaging, from the Council on Cardiovascular Radiology of the American Heart Association. Stroke 2003;34(4):1084–1104.
2. Donahue MJ, Strother MK, Hendrikse J. Novel MRI approaches for assessing cerebral hemodynamics in ischemic cerebrovascular disease. Stroke 2012;43(3):903–915.
3. Amemiya S, Kunimatsu A, Saito N, Ohtomo K. Impaired hemodynamic response in the ischemic brain assessed with BOLD fMRI. Neuroimage 2012;61(3):579–590.
4. Roc AC, Wang J, Ances BM, Liebeskind DS, Kasner SE, Detre JA. Altered hemodynamics and regional cerebral blood flow in patients with hemodynamically significant stenoses. Stroke 2006;37(2):382–387.
5. Biswal B, Yetkin FZ, Haughton VM, Hyde JS. Functional connectivity in the motor cortex of resting human brain using echo-planar MRI. Magn Reson Med 1995;34(4):537–541.
6. Raichle ME, MacLeod AM, Snyder AZ, Powers WJ, Gusnard DA, Shulman GL. A default mode of brain function. Proc Natl Acad Sci U S A 2001;98(2):676–682.
7. Tong Y, Frederick BD. Time lag dependent multimodal processing of concurrent fMRI and near-infrared spectroscopy (NIRS) data suggests a global circulatory origin for low-frequency oscillation signals in human brain. Neuroimage 2010;53(2):553–564.
8. Tong Y, Frederick Bd. Concurrent fNIRS and fMRI processing allows independent visualization of the propagation of pressure waves and bulk blood flow in the cerebral vasculature. Neuroimage 2012;61(4):1419–1427.
9. Fox MD, Zhang D, Snyder AZ, Raichle ME. The global signal and observed anticorre-

lated resting state brain networks. J Neurophysiol 2009;101(6):3270–3283.

10. Carbonell F, Bellec P, Shmuel A. Global and system-specific resting-state fMRI fluctuations are uncorrelated: principal component analysis reveals anti-correlated networks. Brain Connect 2011;1(6):496–510.
11. Biswal B, DeYoe AE, Hyde JS. Reduction of physiological fluctuations in fMRI using digital filters. Magn Reson Med 1996;35(1):107–113.
12. Kiviniemi V, Jauhiainen J, Tervonen O, et al. Slow vasomotor fluctuation in fMRI of anesthetized child brain. Magn Reson Med 2000;44(3):373–378.
13. Kudo K, Sasaki M, Yamada K, et al. Differences in CT perfusion maps generated by different commercial software: quantitative analysis by using identical source data of acute stroke patients. Radiology 2010; 254(1):200–209.
14. Lansberg MG, Lee J, Christensen S, et al. RAPID automated patient selection for reperfusion therapy: a pooled analysis of the Echoplanar Imaging Thrombolytic Evaluation Trial (EPITHET) and the Diffusion and Perfusion Imaging Evaluation for Understanding Stroke Evolution (DEFUSE) Study. Stroke 2011;42(6):1608–1614.
15. Lv Y, Margulies DS, Cameron Craddock R, et al. Identifying the perfusion deficit in acute stroke with resting-state functional magnetic resonance imaging. Ann Neurol 2013;73(1):136–140.
16. Astrup J, Siesjö BK, Symon L. Thresholds in cerebral ischemia: the ischemic penumbra. Stroke 1981;12(6):723–725.
17. Go AS, Mozaffarian D, Roger VL, et al. Heart disease and stroke statistics—2013 update: a report from the American Heart Association. Circulation 2013;127(1):e6–e245.

Original Paper

Neuropsychobiology

Neuropsychobiology 2013;68:197–204
DOI: 10.1159/000355296

Received: September 14, 2012
Accepted after revision: August 26, 2013
Published online: November 1, 2013

# Anterior Cingulate Abnormality as a Neural Correlate of Mismatch Negativity in Schizophrenia

Yayoi K. Hayakawa[a] Eiji Kirino[d] Keigo Shimoji[b] Koji Kamagata[b] Masaaki Hori[b] Kenji Ito[b] Akira Kunimatsu[a] Osamu Abe[c] Kuni Ohtomo[a] Shigeki Aoki[b]

[a]Department of Radiology, Graduate School of Medicine, University of Tokyo, Bunkyo-ku, [b]Department of Radiology, Juntendo University School of Medicine, Hongo, Bunkyo-ku, and [c]Department of Radiology, Nihon University School of Medicine, Tokyo, and [d]Department of Psychiatry, Juntendo University Shizuoka Hospital, Izunokuni, Japan

**Key Words**
Anterior cingulum · Diffusion tensor imaging · Event-related potential · Mismatch negativity · Schizophrenia

**Abstract**
***Background:*** Limbic circuitry, especially the anterior cingulate gyrus, has been implicated in the pathophysiology and cognitive changes of schizophrenia. Previous diffusion tensor imaging studies have demonstrated that the integrity of the anterior cingulum (AC) is abnormal in schizophrenia. However, the relationship between the abnormal AC tract integrity and the pathophysiology of schizophrenia has not been fully studied. ***Methods:*** We performed a voxelwise group comparison of white matter fractional anisotropy (FA) by using tract-based spatial statistics in 9 patients with schizophrenia and 9 matched controls. We then measured FA specifically in the AC by using a tract-specific measurement. The latency and amplitude of the mismatch negativity (MMN) were also evaluated in all subjects. ***Results:*** In patients with schizophrenia, tract-based spatial statistics showed a reduction in FA in broad white matter areas, including the bilateral AC, compared with controls. Tract-specific measurements confirmed the specific reduction of FA in the region of the bilateral AC. The decreased FA in the AC was correlated with prolonged MMN latency in the patient group. ***Conclusion:*** Our study of AC structure and electrophysiological changes in schizophrenia suggest that the disruption of limbic-cortical structural networks may be part of the neural basis underlying the changes in MMN in schizophrenia.


## Introduction

Schizophrenia is a debilitating brain disorder that interferes with cognitive functions and behavior. Many magnetic resonance imaging (MRI) studies of patients with schizophrenia have reported gray matter volume reductions in diverse areas [1–3]. In recent years, diffusion tensor imaging (DTI) studies have reported structural abnormalities in several fiber tracts [3–7], confirming that the structure of the white matter connecting gray matter regions is disrupted. In particular, disruptions between the cingulate gyrus and other regions have been demonstrated [8–11], and these may be associated with the symptoms of schizophrenia [12–14]. However, the functional significance of these structural abnormalities has not been fully investigated.

KARGER

E-Mail karger@karger.com
www.karger.com/nps


0302–282X/13/0684–0197$38.00/0

Yayoi K. Hayakawa
Department of Radiology
Graduate School of Medicine, University of Tokyo
7-3-1, Hongo, Bunkyo-ku, Tokyo 113-8655 (Japan)
E-Mail yayoi-kan@umin.ac.jp

The mismatch negativity (MMN) potential is a commonly used event-related potential (ERP) that has helped to objectively detect cognitive dysfunction in patients with schizophrenia. It is observed as negative voltage fluctuations on the subject's scalp with a peak latency of about 100–250 ms from stimulus onset when the subject perceives deviant stimuli [15–17]. The MMN can be elicited by any occasional discriminable change in a sound sequence, irrespective of the direction of the subject's attention [18]; this process is therefore thought to be automatic and preattentive [19–21]. A reduction in MMN amplitude [22–24] and a prolongation of its peak latency [25] have been shown in patients with schizophrenia. Although several studies have revealed the areas in the gray matter that generate the MMN, predominantly in the temporal auditory cortex and frontal cortex [19, 20], the relationship between the white matter and MMN has not been investigated.

The present study aimed to compare the integrity of the white matter, especially in the anterior cingulum (AC), between patients with schizophrenia and healthy controls. We focus on the AC because its connectivity is thought to be disrupted in schizophrenia, and it is expected to contribute to the regulation of MMN by mediating the interaction between the temporal and frontal cortices. To clarify the functional significance of AC integrity in patients with schizophrenia, we examined the correlation between DTI and MMN. In addition, we investigated the correlation between these structural and physiological changes and clinical symptoms measured by using the Positive and Negative Syndrome Scale (PANSS) [26].

## Materials and Methods

*Participants*

Nine right-handed patients with schizophrenia and 9 healthy controls matched on age, sex, and handedness were recruited. After the subjects had been given a complete description of the study, all provided written informed consent for the protocol, which was approved by the Institutional Review Board of Juntendo University. A 5-component model based on factor analysis of the PANSS [27] was used to assess the patients' clinical symptoms.

*MRI Acquisition*

All MRI scans were obtained at the Juntendo University Hospital by using a 3-tesla MRI unit (Achieva; Philips Medical Systems, Best, the Netherlands) and an 8-channel array receiving head coil for sensitivity-encoding parallel imaging. Regular structural images such as T1-weighted spin-echo images, T2-weighted turbo spin-echo images, and fluid-attenuated inversion recovery images were obtained before the acquisition of diffusion tensor images. DTI was performed by using the spin-echo echo-planar technique. The parameters were as follows: echo time = 70 ms, repetition time = 5,452 ms, voxel size = 1.75 × 1.75 × 3 mm, number of averages = 2, and contiguous axial slices = 50. Images were obtained with both 32-direction diffusion encoding (b = 1,000 s/mm$^2$ for each direction) and no diffusion encoding (b = 0 s/mm$^2$). Scanning time was 7 min 17 s.

*ERP Recording*

Electroencephalography data were recorded in an entirely passive condition, in which the subjects were asked to ignore the stimuli and watch a silent movie projected on an LCD panel. To standardize their level of attention, all subjects were told that they would have to give specific feedback about the movie at the end of the ERP session. A computer with custom-designed software generated acoustic stimuli and controlled both stimulus timing and presentation. Tones were presented binaurally at a constant listening level through tube-connected headphones held in place by a headset. A sound omission paradigm was used where repetitive sequences of a frequent auditory stimulus were occasionally omitted [omission deviant; stimulus onset asynchrony: 136 ms; frequency: 6,547 trials, 3,000 Hz; duration: 35 ms; rise/fall: 0/5 ms; rarity: 53 trials (0.8% of the total); total time: 600 s].

Electroencephalography data were recorded by using a BrainAmp amplifier (Brain Products, Munich, Germany). The BrainCap electrode cap with sintered Ag–AgCl ring electrodes provided 30 electroencephalogram channels, 1 electrocardiogram channel, and 1 electroocular activity channel. The electrodes were positioned according to the extended 10/20 system. During recording, the reference electrode was between the midline frontal electrode (Fz) and the central vertex electrode (Cz) [28], and the ground electrode was the inion position (Iz). MMN was measured from Fz, where it is typically most prominent. Epochs incorporated a 100-ms prestimulus period and a 600-ms poststimulus period. For data analysis, off-line re-referencing of the EEG data was performed to the average recordings of electrodes. All ERP analyses were performed off-line by using the Brain Vision Analyzer Software Package (Brain Products). After scanner artifact removal, artifacts related to pulse (ballistocardiogram), electroocular activity, and gross motion were subtracted from the signal. ERPs to frequent tones were subtracted from ERPs to the omission deviant. In the resulting MMN subtraction waveform, the MMN amplitude was measured as the peak voltage in the 50- to 250-ms interval from event onset (i.e., tone omission), and the MMN peak latency was measured as the time between event onset and MMN peak.

*DTI Analysis*

In an exploratory analysis, we first carried out voxelwise statistical analysis by using tract-based spatial statistics, available as part of the FMRIB software library (FSL) [29]. DTI was preprocessed by using FSL version 4.2.1, including skull stripping and eddy current correction. All subjects' fractional anisotropy (FA) data were aligned into a common space by applying the nonlinear registration tool FNIRT, which uses a b-spline representation of the registration warp field [30]. A mean FA image was provided and thinned to create a mean FA skeleton, which represents the centers of all tracts common to the group. Group comparisons were performed by using Randomise version 2.1 from FSL [31]. Both control versus patient and patient versus control contrasts were tested with 5,000 permutations. We used threshold-free cluster enhancement [32] as implemented within Randomise, which provides the ability to perform cluster-based inferences without setting an ar-

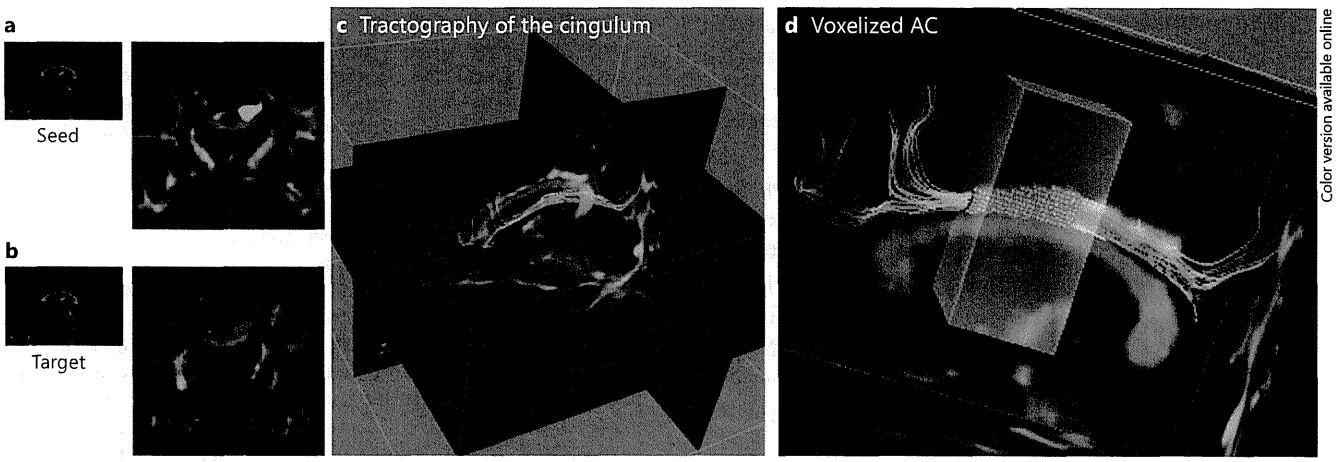


**Fig. 1.** Delineation of the cingulum bundles. **a**, **b** Sagittal (left) and coronal (right) slices of the color map. The 'seed' (blue) and 'target' (pink) ROIs were defined to delineate the cingulum bundle. **c** A 3D view of the extracted cingulum bundle. The tracts between the seed and target were voxelized (**d**). FA values in the voxels were then calculated. See text for details. For colors, see online version.

bitrary cluster-forming threshold. Voxelwise statistical inference was made on the resulting statistic image, and the significance level was set at $p < 0.05$, corrected for the familywise error rate.

As our specific interest was the AC, tract-specific analysis of the 3D diffusion tensor tractograph was performed by using dTV II and VOLUME-ONE software (free software from Masutani, http://www.ut-radiology.umin.jp/people/masutani/dTV.htm) [33] on a Windows PC workstation. In accordance with the two-region-of-interest (ROI) method [33, 34], two ROIs were used to extract the cingulum bundle. The first ROI (the 'seed' ROI) was chosen on the coronal plane anterior to the pons (fig. 1a). The second ROI (the 'target' ROI) was placed on a coronal slice posterior to the genu of the corpus callosum (fig. 1b). After the cingulum bundle had been extracted (fig. 1c), the average values of FA and mean diffusivity of the AC included in the seed and target (fig. 1d) were calculated separately for each hemisphere.

Repeated-measures ANOVA was used to examine the differences on DTI measures, with the group (schizophrenia patients, control subjects) and the side (left and right) as factors. Two-group t tests were carried out to compare MMN amplitude and peak latency between groups. In these analyses, the threshold for statistical significance was set at $p < 0.05$.

Correlation analysis was performed to investigate the relationship between the DTI and MMN measures. Partial correlation coefficients were calculated separately for each group to control for the effects of age and years of education. Unless group-by-side interactions were detected in the group comparison of DTI measures, the average of the DTI measures from both hemispheres was used in the correlation analysis. To maintain an overall alpha value of 0.05, the threshold for statistical significance was set at $p < 0.025$ (Bonferroni's correction, 0.05/2 variables: 1 DTI measure by 2 MMN measures). Furthermore, correlation analysis was performed in the schizophrenia group to explore the association of the 5 components of the PANSS with DTI or MMN measures. To find any possible confounding factors, the DTI measures of each hemisphere were analyzed separately. Taking into account the exploratory nature of the analysis, we set alpha at $p < 0.05$.

**Table 1.** Demographic and clinical information of healthy controls and patients with schizophrenia

| Variable | Controls | Patients | Statistics |
|---|---|---|---|
| Number | 9 | 9 | – |
| Age, years | 29±11 | 36±6.9 | $F(1, 16) = 3.2$, $p > 0.05$ |
| Sex (male/female) | 7/2 | 8/1 | $\chi^2(1) = 0.4$, $p > 0.1$ |
| Handedness (left/right) | 0/9 | 0/9 | – |
| Education, years | 17±1.0 | 13±2.0 | $F(1, 16) = 25$, $p < 0.01$ |
| Mean illness duration, years | – | 13±5.5 | – |
| PANSS | | | |
| Positive | – | 13±7.2 | – |
| Negative | – | 23±10 | – |
| Cognitive | – | 20±7.3 | – |
| Hostility | – | 6.3±2.4 | – |
| Emotional discomfort | – | 10±3.0 | – |

Data are presented as mean ± standard deviation (except for number of subjects, sex and handednes). The values were derived from a 5-component model based on a factor analysis of the PANSS [27].

## Results

### *Participants*

Nine patients with schizophrenia and 9 healthy controls were included in the study. Controls had significantly more years of education than patients, but the groups were otherwise similar (table 1). The grand-average ERP responses of each participant are presented in figure 2.

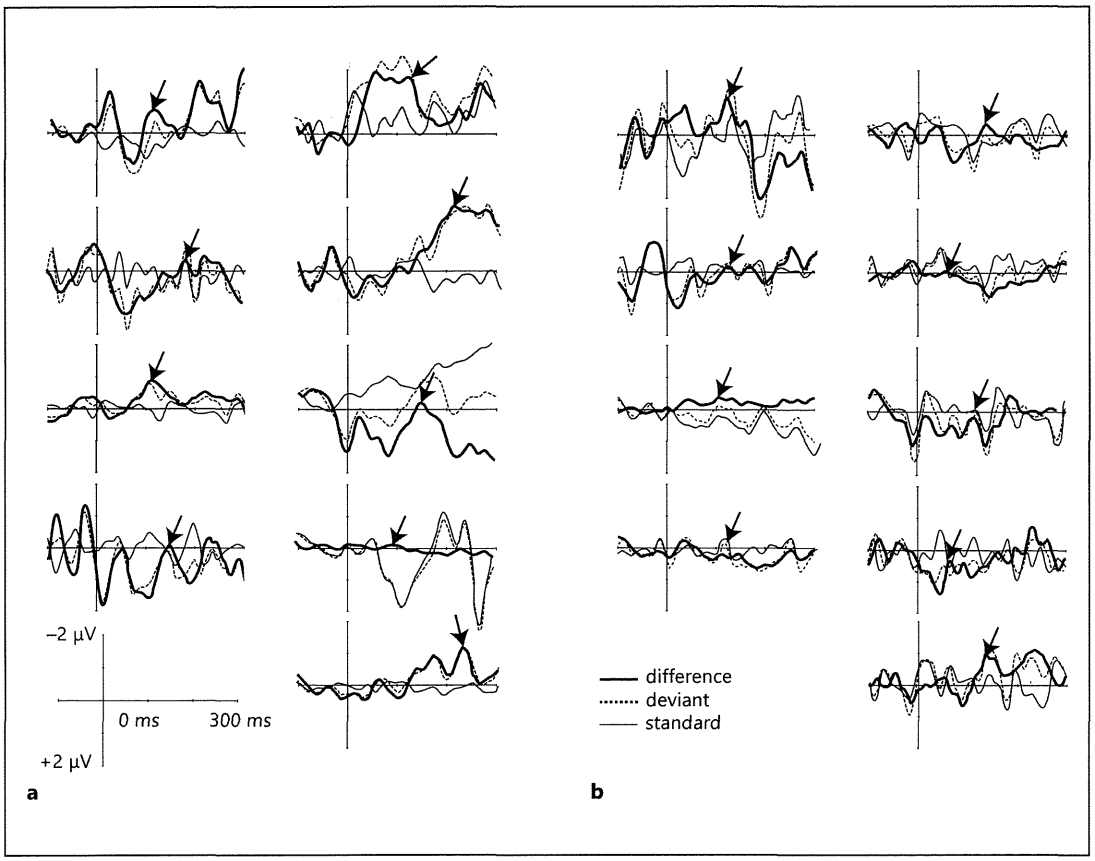


**Fig. 2.** ERP responses of each participant to standard and deviant stimuli. The difference wave was obtained by subtracting the ERP to standards from the ERP to deviants. Arrows indicate mean peak latencies of the MMN. **a** Patients. **b** Controls.

*DTI and MMN Differences between Patients with Schizophrenia and Controls*

Tract-based spatial statistics showed a cluster of significant FA reductions in patients with schizophrenia compared with controls. This cluster included the bilateral anterior cingulate; right posterior cingulate; deep white matter in the frontal, temporal, and parietal lobes; a large portion of the corpus callosum, and the corona radiata (fig. 3). There was no significant cluster of increased FA in patients with schizophrenia.

In the left AC, mean FA values in patients and control subjects were 0.434 (SD = 0.046) and 0.489 (SD = 0.034), respectively; in the right AC, they were 0.404 (SD = 0.027) and 0.424 (SD = 0.022), respectively (fig. 4). Repeated-measures ANOVA demonstrated significant main effects of group [$F(1, 32) = 11.16$, $p = 0.021$] and side [$(F(1, 32) = 17.96$, $p = 0.002$]. The group-by-side interaction did not reach statistical significance. Neither tract-based spatial statistics nor tract-specific analysis revealed group differences in mean diffusivity.

The mean MMN amplitude and peak latency did not differ between controls and patients (table 2).

*Correlation Analysis*

Scatter plots of FA values of the AC measured by tract-specific analysis versus MMN peak latency showed negative relationships between MMN peak latency and FA only in the patient group (fig. 5). A partial correlation analysis to control for the effects of age and education verified the negative correlation between MMN peak latency and mean FA of the AC ($r = -0.95$, $p = 0.001$).

In the patient group, significant correlations were observed between FA in the right AC and the PANSS component of emotional discomfort ($r = -0.73$, $p = 0.027$) and between MMN amplitude and the PANSS component of positive symptoms ($r = 0.93$, $p = 0.002$). After controlling

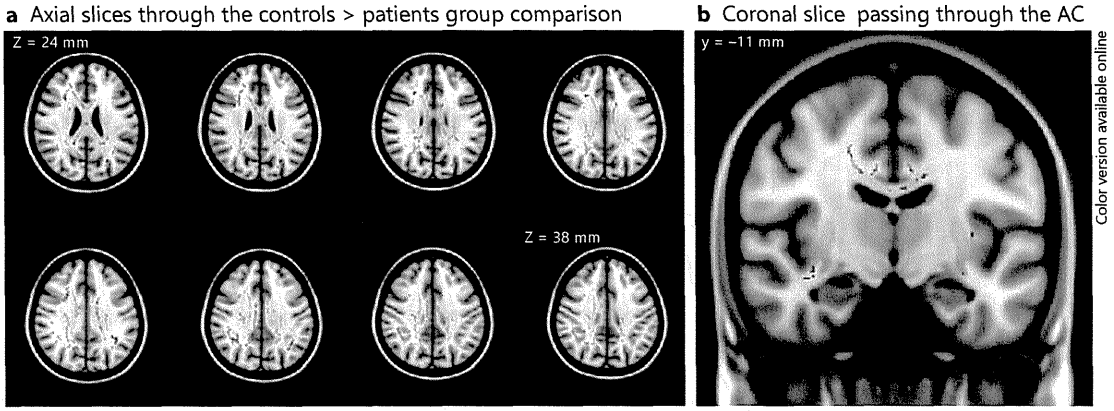


**Fig. 3.** Regions of significant FA reduction in patients with schizophrenia relative to healthy controls (red-yellow, $p < 0.05$, corrected for familywise error). Axial slices from Z = 24 to Z = 38 mm (**a**) and a coronal slice (**b**) show the bilateral anterior cingulum region along with the right posterior cingulum. Left-right orientation is according to the radiological convention.

for the differences on these components, however, the correlations between the FA of each side or the mean FA and the MMN amplitude were not significant.

## Discussion

Relative to controls, patients with schizophrenia showed reduced FA in the AC bilaterally, consistent with previous studies [9–11]. Moreover, the lower FA of the AC was associated with longer MMN latencies in patients with schizophrenia. Some previous studies have associated the cingulum bundle with cognitive dysfunctions in schizophrenia, including social cognition [8], attention and working memory [9, 35], and orienting attention [36]. To our knowledge, this study is the first to examine the FA value and the MMN measures in schizophrenia. The mechanism of MMN has not fully been revealed, but several processes that may interact with each other have been proposed, including the establishment of sensory memory traces [37, 38], change detection [39] when deviant stimuli are compared with maintained representations of the standard stimuli [40, 41], and a switch in attention from an ongoing automatic mode of information processing to top-down controlled attentional processing [42, 43]. The first process is considered to be a sensory process, and the last two are considered to be comparative or cognitive processes [41, 44]. Localization of these components within the cortex has been attempted. In electrophysiological studies, dipole sources for MMN amplitude have been reported in the temporal cortices bilaterally, as well as the right inferior frontal cortex and the left anterior cingulate

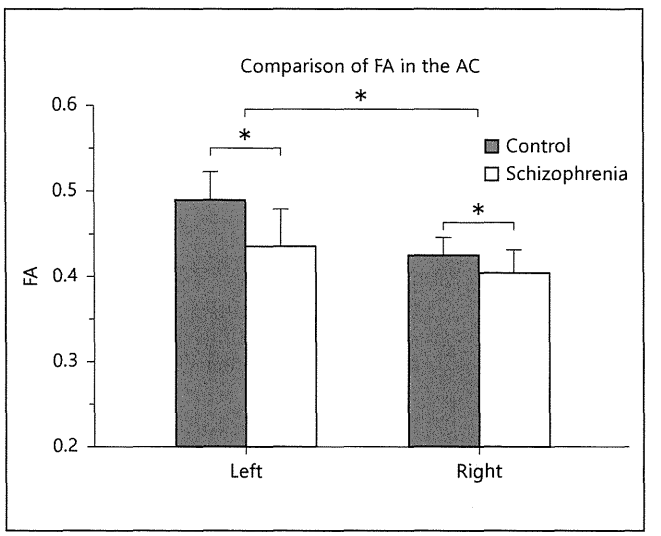


**Fig. 4.** Group and side differences in FA of the AC measured by tract-specific analysis (* $p < 0.05$).

**Table 2.** Mean MMN values in controls and patients with schizophrenia

| | Controls | Patients | Statistics |
|---|---|---|---|
| MMN amplitude, μV | −0.26±0.81 | −1.28±2.4 | $t(16) = -1.7$, $p = 0.11$ |
| MMN latency, ms | 110±31 | 147±50 | $t(16) = -1.9$, $p = 0.08$ |

Data are presented as mean ± standard deviation.



Neuropsychobiology 2013;68:197–204
DOI: 10.1159/000355296

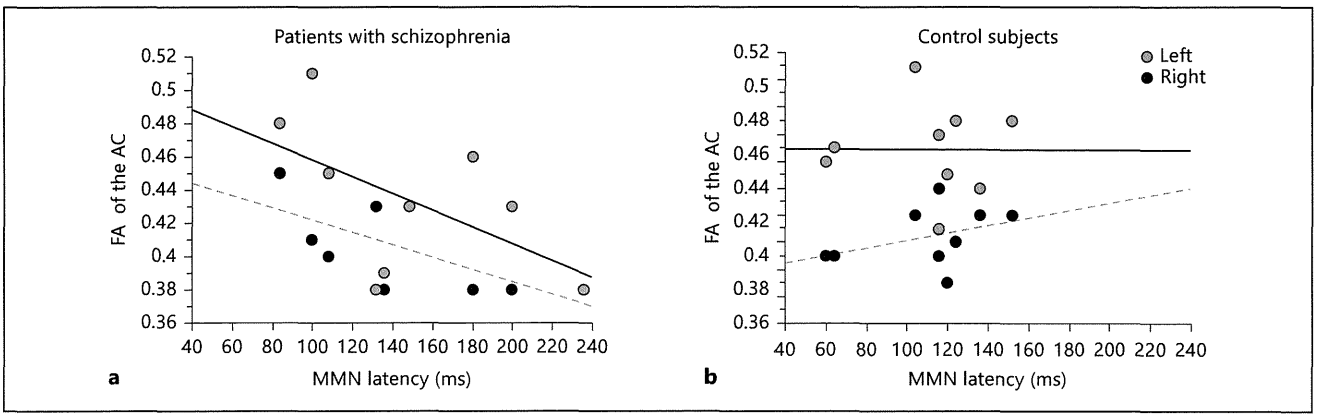


**Fig. 5.** Relationship between FA of the AC measured by tract-specific analysis and MMN peak latency in patients with schizophrenia (**a**) and healthy controls (**b**). Scatter plots show the left and right FA values separately. The least-squares lines for FA values of the right AC are red and those of the left AC are blue. Partial correlation coefficients between MMN peak latency and mean FA of the left and right AC of the patients were $r = -0.95$ ($p = 0.001$). For colors, see online version.

cortex [45, 46]. In a volumetric MRI study, Salisbury et al. [47] found an association between MMN amplitude and a volume reduction in the Heschl gyrus gray matter of the left hemisphere. The auditory cortices may represent sensory memory establishment and updating [41], whereas the inferior frontal and cingulate sources may be part of a region involved in change detection and attention switching [48]. In our study, the lower FA of the AC was associated with prolonged peak latency of the MMN in patients with schizophrenia. The anterior cingulate cortex is a part of a circuit involved in a form of attention. It may be involved in MMN generation that initiates the involuntary switching of attention [49, 50]. In addition, the AC bundle is one of the main white matter tracts connecting the temporal and frontal areas and therefore it might regulate MMN by mediating the interaction between the auditory cortex and frontal area. The reduced integrity of the AC would impair the conflict monitoring and error detection of the anterior cingulate cortex [51, 52], possibly affecting the cognitive processes underlying the MMN. These results may provide evidence of a relationship between white matter integrity and electrophysiological abnormalities of auditory sensory memory in schizophrenia.

Although lower MMN amplitude is thought to be a robust phenomenon in schizophrenic patients [23], we did not detect reduced MMN amplitudes in the current study. In the correlation analysis, MMN amplitude was positively correlated with the PANSS positive symptom component. Previous reports on relationships between MMN and the PANSS have not been consistent [22, 53]. The small sample size in the current study (n = 9 for the patient group) and the heterogeneity between patients suggested by the relatively high standard deviation (7.2 for the PANSS positive symptom component) may have influenced the results. In addition, the number of trials of stimulus omission averaged for MMN was relatively small in this study. It may impair the signal-to-noise ratio and possibly contribute to the lack of a significant group difference.

Because the results were derived from a small sample size, our data should be considered with caution, particularly with regard to the correlation analysis. Although further studies using a larger and less heterogeneous sample group are needed to draw a definitive conclusion, we believe that our study offers a hypothesis about the relationship between white matter integrity and MMN in schizophrenia.

## References


1 Ellison-Wright I, Glahn DC, Laird AR, Thelen SM, Bullmore E: The anatomy of first-episode and chronic schizophrenia: an anatomical likelihood estimation meta-analysis. Am J Psychiatry 2008;165:1015–1023.

2 Flashman LA, McAllister TW, Johnson SC, Rick JH, Green RL, Saykin AJ: Specific frontal lobe subregions correlated with unawareness of illness in schizophrenia: a preliminary study. J Neuropsychiatry Clin Neurosci 2001; 13:255–257.

3 Moriya J, Kakeda S, Abe O, Goto N, Yoshimura R, Hori H, Ohnari N, Sato T, Aoki S, Ohtomo K, Nakamura L, Korogi Y: Gray and white matter volumetric and diffusion tensor imaging (DTI) analyses in the early stage of first-episode schizophrenia. Schizophr Res 2010; 116:196–203.

4 Abdul-Rahman MF, Qiu A, Sim K: Regionally specific white matter disruptions of fornix and cingulum in schizophrenia. PloS One 2011;6:e18652.
5 Jeong B, Wible CG, Hashimoto R, Kubicki M: Functional and anatomical connectivity abnormalities in left inferior frontal gyrus in schizophrenia. Hum Brain Mapp 2009;30:4138–4151.
6 Kubicki M, McCarley R, Westin CF, Park HJ, Maier S, Kikinis R, Jolesz FA, Shenton ME: A review of diffusion tensor imaging studies in schizophrenia. J Psychiatr Res 2007;41:15–30.
7 Park HJ, Westin CF, Kubicki M, Maier SE, Niznikiewicz M, Baer A, Frumin M, Kikinis R, Jolesz FA, McCarley RW, Shenton ME: White matter hemisphere asymmetries in healthy subjects and in schizophrenia: a diffusion tensor MRI study. NeuroImage 2004;23:213–223.
8 Fujiwara H, Namiki C, Hirao K, Miyata J, Shimizu M, Fukuyama H, Sawamoto N, Hayashi T, Murai T: Anterior and posterior cingulum abnormalities and their association with psychopathology in schizophrenia: a diffusion tensor imaging study. Schizophr Res 2007;95:215–222.
9 Kubicki M, Westin CF, Nestor PG, Wible CG, Frumin M, Maier SE, Kikinis R, Jolesz FA, McCarley RW, Shenton ME: Cingulate fasciculus integrity disruption in schizophrenia: a magnetic resonance diffusion tensor imaging study. Biol Psychiatry 2003;54:1171–1180.
10 Sun Z, Wang F, Cui L, Breeze J, Du X, Wang X, Cong Z, Zhang H, Li B, Hong N, Zhang D: Abnormal anterior cingulum in patients with schizophrenia: a diffusion tensor imaging study. Neuroreport 2003;14:1833–1836.
11 Wang F, Sun Z, Cui L, Du X, Wang X, Zhang H, Cong Z, Hong N, Zhang D: Anterior cingulum abnormalities in male patients with schizophrenia determined though diffusion tensor imaging. Am J Psychiatry 2004;161:573–575.
12 Cohen RA, Kaplan RF, Moser DJ, Jenkins MA, Wilkinson H: Impairments of attention after cingulotomy. Neurology 1999;53:819–824.
13 Manoach DS, Ketwaroo GA, Polli FE, Thakkar KN, Barton JJ, Goff DC, Fischl B, Vangel M, Tuch DS: Reduced microstructural integrity of the white matter underlying anterior cingulate cortex is associated with increased saccadic latency in schizophrenia. Neuroimage 2007;37:599–610.
14 Segal D, Haznedar MM, Hazlett EA, Entis JJ, Newmark RE, Torosjan Y, Schneiderman JS, Friedman J, Chu KW, Tang CY, Buchsbaum MS, Hof PR: Diffusion tensor anisotropy in the cingulate gyrus in schizophrenia. Neuroimage 2010;50:357–365.
15 Näätänen R: The mismatch negativity: a powerful tool for cognitive neuroscience. Ear Hear 1995;16:6–18.
16 Näätänen R, Alho K: Mismatch negativity – A unique measure of sensory processing in audition. Int J Neurosci 1995;80:317–337.
17 Sinkkonen J, Tervaniemi M: Towards optimal recording and analysis of the mismatch negativity. Audiol Neurootol 2000;5:235–246.
18 Rinne T, Alho K, Ilmoniemi RJ, Virtanen J, Näätänen R: Separate time behaviors of the temporal and frontal mismatch negativity sources. Neuroimage 2000;12:14–19.
19 Näätänen R, Kujala T, Winkler I: Auditory processing that leads to conscious perception: a unique window to central auditory processing opened by the mismatch negativity and related responses. Psychophysiology 2011;48:4–22.
20 Näätänen R, Kujala T, Kreegipuu K, Carlson S, Escera C, Baldeweg T, Ponton C: The mismatch negativity: an index of cognitive decline in neuropsychiatric and neurological diseases and in ageing. Brain 2011;134:3435–3453.
21 Näätänen R, Kujala T, Escera C, Baldeweg T, Kreegipuu K, Carlson S, Ponton C: The mismatch negativity (MMN) – A unique window to disturbed central auditory processing in ageing and different clinical conditions. Clin Neurophysiol 2012;123:424–458.
22 Rosburg T, Haueisen J, Kreitschmann-Andermahr I: The dipole location shift within the auditory evoked neuromagnetic field components N100m and mismatch negativity (MMNm). Clin Neurophysiol 2004;115:906–913.
23 Michie PT: What has MMN revealed about the auditory system in schizophrenia? Int J Psychophysiol 2001;42:177–194.
24 Näätänen R, Kähkönen S: Central auditory dysfunction in schizophrenia as revealed by the mismatch negativity (MMN) and its magnetic equivalent MMNm: a review. Int J Neuropsychopharmacol 2009;12:125–135.
25 Kathmann N, Wagner M, Rendtorff N, Engel RR: Delayed peak latency of the mismatch negativity in schizophrenics and alcoholics. Biol Psychiatry 1995;37:754–757.
26 Kay SR, Fiszbein A, Opler LA: The positive and negative syndrome scale (PANSS) for schizophrenia. Schizophr Bull 1987;13:261–276.
27 Bell MD, Lysaker PH, Beam-Goulet JL, Mistein RM, Lindenmeyer JP: Five-component model of schizophrenia: assessing the factorial invariance of the positive and negative syndrome scale. Psychiatry Res 1994;52:295–303.
28 Laufs H, Krakow K, Sterzer P, Eger E, Beyerle A, Kleinschmidt A: Electroencephalographic signatures of attentional and cognitive default modes in spontaneous brain activity fluctuations. Proc Natl Acad Sci USA 2003;100:11053–11058.
29 Smith SM, Jenkinson M, Johansen-Berg H, Rueckert D, Nichols TE, Mackay CE, Watkins KE, Ciccarelli O, Cader MZ, Matthews PM, Behrens TE: Tract-based spatial statistics: voxelwise analysis of multi-subject diffusion data. Neuroimage 2006;31:1487–1505.
30 Rueckert D, Sonoda L, Hayes C, Hill DL, Leach MO, Hawkes DJ: Nonrigid registration using free-form deformations: application to breast MR images. IEEE Trans Med Imaging 1999;18:712–721.
31 Nichols TE, Holmes AP: Nonparametric permutation tests for functional neuroimaging: a primer with examples. Hum Brain Mapp 2001;15:1–25.
32 Smith SM, Nichols TE: Threshold-free cluster enhancement: addressing problems of smoothing, threshold dependence and localisation in cluster inference. Neuroimage 2009;44:83–98.
33 Masutani Y, Aoki S, Abe O, Hayashi N, Otomo K: MR diffusion tensor imaging: recent advance and new techniques for diffusion tensor visualization. Eur J Radiol 2003;46:53–66.
34 Kunimatsu A, Aoki S, Masutani Y, Abe O, Hayashi N, Mori H, Masumoto T, Ohtomo K: The optimal trackability threshold of fractional anisotropy for diffusion tensor tractography of the corticospinal tract. Magn Reson Med Sci 2004;3:11–17.
35 Takei K, Yamasue H, Abe O, Yamada H, Inoue H, Suga M, Muroi M, Sasaki H, Aoki S, Kasai K: Structural disruption of the dorsal cingulum bundle is associated with impaired Stroop performance in patients with schizophrenia. Schizophr Res 2009;114:119–127.
36 Nestor PG, Kubicki M, Spencer KM, Niznikiewicz M, McCarley RW, Shenton ME: Attentional networks and cingulum bundle in chronic schizophrenia. Schizophr Res 2007;90:308–315.
37 Paavilainen P, Alho K, Reinikainen K, Sams M, Näätänen R: Right hemisphere dominance of different mismatch negativities. Electroencephalogr Clin Neurophysiol 1991;78:466–479.
38 Jacobsen T, Schröger E: Is there pre-attentive memory-based comparison of pitch? Psychophysiology 2001;38:723–727.
39 Beck DM, Rees G, Frith CD, Lavie N: Neural correlates of change detection and change blindness. Nat Neurosci 2001;4:645–650.
40 Javitt DC, Doneshka P, Zylberman I, Ritter W, Vaughan HG Jr: Impairment of early cortical processing in schizophrenia: an event-related potential confirmation study. Biol Psychiatory 1993;33:513–519.
41 Halgren E, Sherfey J, Irimia A, Dale AA, Marinkovic K: Sequential temporo-fronto-temporal activation during monitoring of the auditory environment for temporal patterns. Hum Brain Mapp 2011;32:1260–1276.
42 Schröger E: A neural mechanism for involuntary attention shifts to changes in auditory stimulation. J Cogn Neurosci 1996;8:527–539.
43 Escera C, Alho K, Winkler I, Näätänen R: Neural mechanisms of involuntary attention to acoustic novelty and change. J Cogn Neurosci 1998;10:590–604.

44 Kasai K, Nakagome K, Itoh K, Koshida I, Hata A, Iwanami A, Fukuda M, Kato N: Impaired cortical network for preattentive detection of change in speech sounds in schizophrenia: a high-resolution event-related potential study. Am J Psychiatry 2002;159:546–553.
45 Jemel B, Achenbach C, Müller B, Röpcke B, Oades RD: Mismatch negativity results from bilateral asymmetric dipole sources in the frontal and temporal lobes. Brain Topogr 2002;15:13–27.
46 Valkonen-Korhonen M, Purhonen M, Tarkka IM, Sipilä P, Partanen J, Karhu J, Lehtonen J: Altered auditory consciousness in acutely psychotic, never-medicated first-episode patients. Cogn Brain Res 2003;17:747–758.
47 Salisbury DF, Kuroki N, Kasai K, Shenton ME, McCarley RW: Progressive and interrelated functional and structural evidence of post-onset brain reduction in schizophrenia. Arch Gen Psychiatry 2007;64:521–529.
48 Oknina LB, Wild-Wall N, Oades RD, Juran SA, Röpcke B, Pfueller U, Weisbrod M, Chan E, Chen EY: Frontal and temporal sources of mismatch negativity in healthy controls, patients at onset of schizophrenia in adolescence and others at 15 years after onset. Schizophr Res 2005;76:25–41.
49 Giard MH, Perrin F, Pernier J, Bouchet P: Brain generators implicated in the processing of auditory stimulus deviance: a topographic event-related potential study. Psychophysiology 1990;27:627–640.
50 Molholm S, Martinez A, Ritter W, Javitt DC, Foxe JJ: The neural circuitry of pre-attentive auditory change-detection: an fMRI study of pitch and duration mismatch negativity generators. Cereb Cortex 2005;15:545–551.
51 Carter CS, Braver TS, Barch DM, Botvinick MM, Noll D, Cohen JD: Anterior cingulate cortex, error detection, and the online monitoring of performance. Science 1998;280:747–749.
52 Brazdil M, Roman R, Falkenstein M, Daniel P, Jurák P, Rektor I: Error processing – Evidence from intracerebral ERP recordings. Exp Brain Res 2002;146:460–466.
53 Jordanov T, Popov T, Weisz N, Elbert T, Paul-Jordanov I, Rockstroh B: Reduced mismatch negativity and increased variability of brain activity in schizophrenia. Clin Neurophysiol 2011;122:2365–2374.

OPEN ACCESS Freely available online

PLOS | ONE

# Altered Network Topologies and Hub Organization in Adults with Autism: A Resting-State fMRI Study

**Takashi Itahashi[1], Takashi Yamada[2], Hiromi Watanabe[2], Motoaki Nakamura[2,3], Daiki Jimbo[4], Seiji Shioda[4], Kazuo Toriizuka[1], Nobumasa Kato[2], Ryuichiro Hashimoto[2,5]***

**1** Department of Pharmacognosy and Phytochemistry, Showa University School of Pharmacy, Tokyo, Japan, **2** Department of Psychiatry, Showa University School of Medicine, Tokyo, Japan, **3** Kinko Hospital, Kanagawa Psychiatric Center, Kanagawa, Japan, **4** Department of Anatomy, Showa University School of Medicine, Tokyo, Japan, **5** Department of Language Sciences, Graduate School of Humanities, Tokyo Metropolitan University, Tokyo, Japan

## Abstract

Recent functional magnetic resonance imaging (fMRI) studies on autism spectrum condition (ASC) have identified dysfunctions in specific brain networks involved in social and non-social cognition that persist into adulthood. Although increasing numbers of fMRI studies have revealed atypical functional connectivity in the adult ASC brain, such functional alterations at the network level have not yet been fully characterized within the recently developed graph-theoretical framework. Here, we applied a graph-theoretical analysis to resting-state fMRI data acquired from 46 adults with ASC and 46 age- and gender-matched controls, to investigate the topological properties and organization of autistic brain network. Analyses of global metrics revealed that, relative to the controls, participants with ASC exhibited significant decreases in clustering coefficient and characteristic path length, indicating a shift towards randomized organization. Furthermore, analyses of local metrics revealed a significantly altered organization of the hub nodes in ASC, as shown by analyses of hub disruption indices using multiple local metrics and by a loss of "hubness" in several nodes (e.g., the bilateral superior temporal sulcus, right dorsolateral prefrontal cortex, and precuneus) that are critical for social and non-social cognitive functions. In particular, local metrics of the anterior cingulate cortex consistently showed significant negative correlations with the Autism-Spectrum Quotient score. Our results demonstrate altered patterns of global and local topological properties that may underlie impaired social and non-social cognition in ASC.

**Citation:** Itahashi T, Yamada T, Watanabe H, Nakamura M, Jimbo D, et al. (2014) Altered Network Topologies and Hub Organization in Adults with Autism: A Resting-State fMRI Study. PLoS ONE 9(4): e94115. doi:10.1371/journal.pone.0094115

**Editor:** Satoru Hayasaka, Wake Forest School of Medicine, United States of America

**Received** January 6, 2014; **Accepted** March 12, 2014; **Published** April 8, 2014



**Funding:** A part of this study is the result of "Development of BMI Technologies for Clinical Application" carried out under the Strategic Research Program for Brain Sciences by the Ministry of Education, Culture, Sports, Science and Technology of Japan. This work was also supported by the Japan Society for the Promotion of Science (JSPS) Grant-in-Aid for Young Scientists (B) (25870738 to T.I.) and by a Grant-in-Aid for Scientific Research on Innovative Areas (23118003; Adolescent Mind & Self-Regulation to R.H.) from the Ministry of Education, Culture, Sports, Science, and Technology of Japan. The funders had no role in study design, data collection and analysis, decision to publish, or preparation of the manuscript.

**Competing Interests:** The authors have declared that no competing interests exist.

* E-mail: dbridges50@gmail.com

## Introduction

Autism spectrum condition (ASC) has been characterized by impairments in social and communication skills, combined with repetitive and restricted behavior. However, this spectrum comprises a range of heterogeneous populations with varying degrees of severity. The debates surrounding the precise definition of its core symptoms, as well as the choice of the term for characterizing this spectrum (i.e., "disorder" or "condition"), have not been settled even in the latest version of the American Psychiatry Association's Diagnostic and Statistical Manual of Mental Disorders-Fifth Edition (DSM-V) has been published [1]. In an effort to reveal functional brain alterations underlying the clinical symptoms of ASC, an increasing number of functional magnetic resonance imaging (fMRI) studies have recently examined intrinsic activity in the absence of externally imposed tasks. Such resting-state fMRI (rs-fMRI) studies have found atypical intrinsic connectivity in ASC (for overview, see [2]): for instance, under-connectivity within a default mode network [3,4], and over- and under-connectivity between many pairs of brain regions [5,6]. These abnormal functional interactions between distributed brain areas lend support to the hypothesis that brain abnormalities in ASC can best be understood as a network disorder [7].

In neuroscience research, network studies (connectomics) of the human brain are becoming the key to understanding brain functions and mechanisms of neuropathological disorders [8]. In particular, advances in graph-theoretical analysis of rs-fMRI data have provided a new perspective on the functional organization of the human brain. This approach enables the representation of the whole brain as a large-scale network composed of nodes (brain regions) and edges (connections between nodes), and allows the examination of the topological properties of the network [9]. At the network level, for example, a small-world network is characterized by high clustering and short characteristic path length [10], which is a hallmark of the human brain network [11,12]. At the nodal level, the degree of a node quantifies the connectedness of the node with the rest of nodes in a network and therefore is useful in identifying highly connected nodes (i.e., hubs) that may play critical roles in information integration [13]. Several studies have identified functional hubs, particularly along the midline cortical regions (e.g., the supplementary motor area and precuneus) in neurotypical individuals [14–17]. While network